3-20-1998

Rainbow Scattering by a Cylinder with a Nearly Elliptical Cross Section

Charles L. Adler

James A. Lock
Cleveland State University, j.lock@csuohio.edu

Bradley R. Stone

Publisher's Statement

Original Citation

Adler, Charles L., James A. Lock, and Bradley R. Stone. "Rainbow Scattering by a Cylinder with a Nearly Elliptical Cross Section." *Applied Optics* 37 (1998): 1540-1550.

Repository Citation

Rainbow scattering by a cylinder with a nearly elliptical cross section

Charles L. Adler, James A. Lock, and Bradley R. Stone

We both theoretically and experimentally examine the behavior of the first- and the second-order rainbows produced by a normally illuminated glass rod, which has a nearly elliptical cross section, as it is rotated about its major axis. We decompose the measured rainbow angle, taken as a function of the rod's rotation angle, into a Fourier series and find that the rod's refractive index, average ellipticity, and deviation from ellipticity are encoded primarily in the $m = 0, 2, 3$ Fourier coefficients, respectively. We determine these parameters for our glass rod and, where possible, compare them with independent measurements. We find that the average ellipticity of the rod agrees well with direct measurements, but that the rod's diameter inferred from the spacing of the supernumeraries of the first-order rainbow is significantly larger than that obtained by direct measurement. We also determine the conditions under which the deviation of falling water droplets from an oblate spheroidal shape permits the first few supernumeraries of the second-order rainbow to be observed in a rain shower.

OCIS codes: 010.1310, 080.1510, 290.3030, 290.5820.

1. Introduction

Historically the study of rainbows produced by the interaction of light with a long dielectric rod or fiber has received less attention than has the study of rainbows produced by a sphere or spheroid. In the 1860's, Billet observed glare spots corresponding to the first 19 rainbows in a thin column of falling water,[1] and in the first decade of this century, Möbius examined the first-order rainbow of a number of glass rods that had a circular or elliptical cross section.[2,3] More recently, the angular positions of the first-order rainbow and its supernumeraries have been used to determine both the refractive index and the diameter of unclad optical fibers.[4] Each of these experiments used normally incident light. For diagonal incidence, the first-order rainbow of a circular-cross-section rod and the rainbow's extinction transition have also been studied.[5–7] In addition, electromagnetic scattering theory has recently been extended from the cases of cylinders that have a circular[8–10] or elliptical[11,12] cross section to a cylinder whose cross section contains small deviations from an elliptical shape.[13] In this extension of the theory, the cylinder cross section is expressed in polar coordinates as a Fourier series and a plane wave or Gaussian laser beam is normally incident.

When a glass rod or fiber is manufactured, its cross section is rarely perfectly circular, or even perfectly elliptical. In this case the cylinder is said to have a nonelliptical cross section (the term is not to be confused with zero ellipticity, i.e., a circular cylinder). We show here that the sensitive dependence of the rainbow angle on both the shape of the cylinder cross section and the rotation angle of the cylinder allows the rainbow angle to be used to obtain an estimate of the cross-sectional shape.

Certain symmetries of a rod's cross section may easily be determined by rotation of the rod about its major axis and examination of the scattering angle of the first- or the second-order rainbow for normally incident light. If the rainbow angle remains constant as the rod is rotated, the rod's cross section is circular. If it varies in a periodic fashion as the rod is rotated through multiples of 180°, the cross section has twofold symmetry (i.e., it has two symmetry axes at 90° with respect to each other). An ellipse is one of the simplest figures possessing this symmetry. If, however, the rainbow angle varies in a periodic fash-

When this work was performed, the authors were with the Department of Physics, Cleveland State University, Cleveland, Ohio 44115. C. L. Adler's permanent address is the Department of Physics, St. Mary's College of Maryland, St. Mary's City, Maryland 20686. B. R. Stone's permanent address is the Department of Electrical Engineering, The University of Dayton, Dayton, Ohio 45469.

Received 20 June 1997; revised manuscript received 12 November 1997.

0003-6935/98/091540-11$15.00/0

ion as the rod is rotated through only multiples of 360°, the cross section has a more complicated shape that lacks twofold symmetry.

In this paper we examine rainbow formation for a special class of nonelliptical-cross-section cylinders in the short-wavelength limit by using geometric ray methods rather than rigorous electromagnetic theory, and we describe a procedure for estimating the shape of a cylinder's cross section from observations of the rainbow angle taken as a function of the cylinder's rotation angle ξ for normal plane-wave incidence. In Section 2 the cylinder's cross section is modeled as two half-ellipses with different aspect ratios joined smoothly along their common major axis. This is one of the simplest shapes possessing only a single symmetry axis, and the expressions describing ray propagation inside such a cylinder are relatively straightforward. For this model system, we numerically compute the far-zone scattering angle of the first- and the second-order rainbows as a function of ξ and find that the results are readily interpretable when expressed as a Fourier series in ξ. We find the second-order rainbow angle to be much more sensitive to deviations from ellipticity for the refractive index of glass than is the first-order rainbow angle. In Section 3 we experimentally measure the first- and the second-order rainbow angles produced by a plane wave normally incident upon a glass rod whose cross section contains small deviations from ellipticity. We then fit the two-half-ellipse cross-section model to the experimental data by matching the largest Fourier coefficients of the experimental data with the theoretical coefficients obtained in Section 2. We also infer the rod's average diameter from the spacing of the supernumeraries of the first-order rainbow. In Section 4 we determine the conditions under which deviations from ellipticity in the vertical cross section of falling water droplets in a rain shower[14] permit the observation of the first few supernumeraries at the topmost portion of the second-order rainbow.[15–17] Last, in Section 5 we discuss our results.

2. Scattering by a Two-Half-Ellipse Cross-Section Cylinder in Ray Theory

We consider a long homogeneous dielectric cylinder of refractive index n and whose cross section is modeled by

$$\frac{x'^2}{a^2}+\frac{y'^2}{b_1^2}=1 \qquad \text{for } y'\geq 0,$$

$$\frac{x'^2}{a^2}+\frac{y'^2}{b_2^2}=1 \qquad \text{for } y'<0, \tag{1}$$

where the $x'y'z'$ coordinate system is attached to the cylinder. The cylinder's main axis coincides with the z' axis. The two half-ellipses have a common semimajor axis a, differing semiminor axes b_1 and b_2, and are smoothly joined together at $x'=\pm a$, $y'=0$, as is shown in Fig. 1(a). The first derivative of the cross section is continuous at the join points R and L, but the second derivative is discontinuous there.

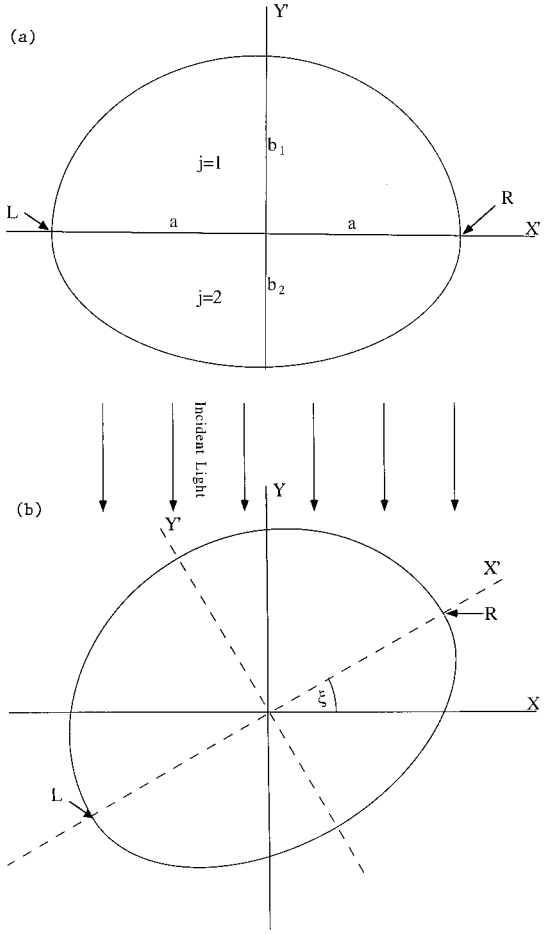

Fig. 1. (a) Cylinder has a cross section consisting of two half-ellipses denoted by the index $j=1, 2$ joined smoothly at the points R and L. The length of the common semimajor axis of the two half-ellipses is a, and the length of their differing semiminor axes are b_1 and b_2. The $x'y'z'$ coordinate system is attached to the cylinder. (b) The cylinder is rotated by an angle ξ about the z' axis. Incident light rays propagate in the $-y$ direction of a fixed laboratory coordinate system.

The cylinder is rotated about the z' axis, as is shown in Fig. 1(b), so that the x' axis makes an angle ξ with the x axis of a fixed xyz laboratory coordinate system whose z axis coincides with the z' axis. The surface of the rotated cylinder is given in the laboratory coordinate system by

$$y=-\beta_j x \pm \alpha_j (A_j^2 - x^2)^{1/2}, \tag{2}$$

where

$$A_j^2=(b_j^2/a^2)\sin^2\xi+\cos^2\xi, \tag{3}$$

$$\alpha_j=(b_j/a)/A_j^2, \tag{4}$$

$$\beta_j=(b_j^2/a^2-1)\sin\xi\cos\xi/A_j^2, \tag{5}$$

where the index $j=1, 2$ denotes the two half-ellipses in Eq. (1). We consider a family of parallel light rays traveling in the $-y$ direction and incident upon the cylinder. For this geometry the upper sign in Eq. (2) corresponds to the illuminated side of the cylinder

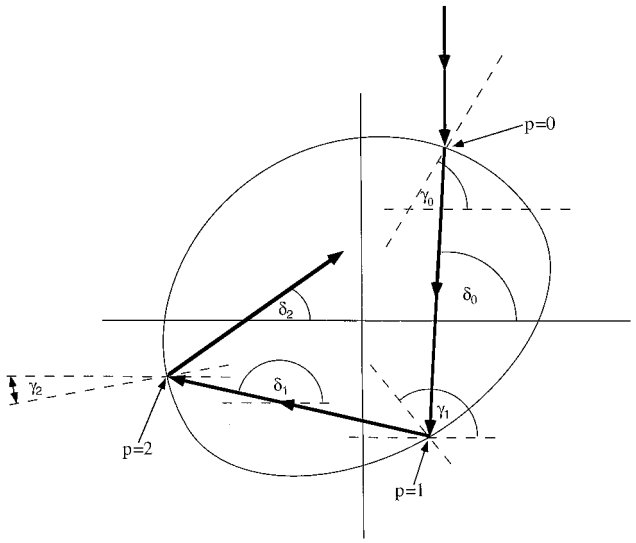

Fig. 2. Angles γ_p of the normal to the surface and the angles δ_p of the interior rays for the $0 \le p \le 2$ interactions of a light ray with the surface.

and the lower sign corresponds to the shadowed side. When describing the scattered rays, we employ the usual notation in which the initial interaction of a ray with the illuminated side of the cylinder is numbered by $p = 0$ and successive internal reflections at the surface are numbered by $p \ge 1$. The p interaction occurs at the coordinates (x_p, y_p). The rays that form the first-order rainbow and its supernumeraries exit the cylinder at the $p = 2$ interaction, and the rays that form the second-order rainbow and its supernumeraries exit at the $p = 3$ interaction.

With this convention, the normal to the cylinder surface at (x_p, y_p) makes an angle γ_p with respect to the positive x axis, where

$$\tan \gamma_p = \frac{A_j^2 - x_p^2}{x_p y_p + \beta_j A_j^2}. \tag{6}$$

The angle that a ray inside the cylinder between the p and the $p + 1$ interactions makes with the positive x axis is δ_p, where

$$\delta_0 = \gamma_0 + \arcsin[(\cos \gamma_0)/n], \tag{7}$$

$$\delta_1 = 2\gamma_1 - \delta_0, \tag{8}$$

$$\delta_2 = 2\gamma_2 - \delta_1 - \pi. \tag{9}$$

The angles γ_p and δ_p for $0 \le p \le 2$ are shown in Fig. 2 for a representative ray. Given (x_p, y_p) and δ_p, we obtain the coordinates (x_{p+1}, y_{p+1}) by substituting Eq. (2) for y_{p+1} into

$$\tan \delta_p = (y_{p+1} - y_p)/(x_{p+1} - x_p) \tag{10}$$

and solving the resulting quadratic equation in x_{p+1}. The roots of the quadratic give x_p, the location on the surface that the ray has just left, and x_{p+1}, the location on the surface that the ray is going to. Because we assume that the cylinder cross section deviates from circularity by only a few percent, the root of the quadratic that produced x_{p+1} in the circular-cross-section limit is chosen. The resulting value of x_{p+1} is then substituted back into Eq. (10) to obtain y_{p+1}. We begin tracing a ray from one interaction with the cylinder surface to the next by specifying (x_p, y_p), calculating γ_p by using Eq. (6), calculating δ_p by using Eqs. (7)–(9), and then calculating (x_{p+1}, y_{p+1}) by using Eq. (10) and the quadratic procedure. This process is repeated until the desired number of internal reflections has been achieved.

The deviation angle of rays exiting the cylinder at the $p = 2$ interaction is

$$\theta_2 = 3\pi/2 + \arcsin[n \sin(\gamma_2 - \delta_1)] - \gamma_2, \tag{11}$$

and the deviation angle of rays exiting at the $p = 3$ interaction is

$$\theta_3 = 3\pi/2 + \arcsin[n \sin(\gamma_3 - \delta_2)] - \gamma_3. \tag{12}$$

Equivalent expressions for the deviation angle were derived in Ref. 18. The first- and the second-order rainbow angles, $\theta_2^R(\xi)$ and $\theta_3^R(\xi)$, respectively, are the relative minima of Eqs. (11) and (12) taken as a function of x_0 for a given cylinder rotation angle ξ. The Descartes deviation angle θ_p^D of the $p - 1$-order rainbow for a circular-cross-section cylinder is given by

$$\cos \phi_i^D = \left(\frac{n^2 - 1}{p^2 - 1}\right)^{1/2}, \tag{13}$$

$$\sin \phi_t^D = (1/n)\sin \phi_i^D, \tag{14}$$

$$\theta_p^D = (p - 1)\pi + 2\phi_i^D - 2p\phi_t^D. \tag{15}$$

Of special concern in ray-tracing calculations with the two-half-ellipse cross-section model is the fact that at each interaction of a ray with the cylinder surface, a determination must be made as to whether the interaction occurs on the $j = 1$ half-ellipse or on the $j = 2$ half-ellipse. This determination was made in the following way. In the laboratory coordinate system, the two join points of the half-ellipses R and L are located at

$$x_R = a \cos \xi, \qquad x_L = -a \cos \xi,$$
$$y_R = a \sin \xi, \qquad y_L = -a \sin \xi. \tag{16}$$

The $p = 0$ interaction occurs on the $j = 1$ half-ellipse if $x_0 \le x_R$ when $0° \le \xi \le 180°$ and if $x_0 > x_L$ when $180° \le \xi \le 360°$. It occurs on the $j = 2$ half-ellipse if $x_0 > x_R$ when $0° \le \xi \le 180°$ and if $x_0 \le x_L$ when $180° < \xi \le 360°$. For $p \ge 1$, the value of j changes from one interaction with the surface to the next when the ray traveling inside the cylinder between the two interaction points crosses the join line of the half-ellipses between R and L.

For a cylinder whose cross section is exactly elliptical, Eqs. (2)–(12) may be Taylor-series expanded in powers of the ellipticity defined by

$$\epsilon = (b/a) - 1, \tag{17}$$

and the relative minima of Eqs. (11) and (12) may be determined analytically. In order to test the correctness of Eqs. (2)–(12), we performed such a Taylor-series expansion and found that

$$\theta_2^R(\xi) = \theta_2^D - 8\epsilon \sin \phi_t^D \cos^3 \phi_t^D \times \cos(2\xi + \theta_2^D) + O(\epsilon^2), \quad (18)$$

$$\theta_3^R(\xi) = \theta_3^D + 32\epsilon \sin \phi_t^D \cos^3 \phi_t^D \times \cos 2\phi_t^D \cos(2\xi + \theta_3^D) + O(\epsilon^2), \quad (19)$$

in agreement with the published first order in ϵ approximation to the rainbow angles for an elliptical-cross-section cylinder.[2,3,16]

In order to examine the sensitivity of the first- and the second-order rainbow angles on both the average ellipticity and the deviation from ellipticity of the cylinder cross section, the rainbow angles $\theta_2^R(\xi)$ and $\theta_3^R(\xi)$ are Fourier transformed by means of

$$\theta_2^R(\xi) = E_0 + \sum_{m=1}^{\infty} E_m \cos(m\xi) + \sum_{m=1}^{\infty} F_m \sin(m\xi), \quad (20)$$

$$\theta_3^R(\xi) = G_0 + \sum_{m=1}^{\infty} G_m \cos(m\xi) + \sum_{m=1}^{\infty} H_m \sin(m\xi). \quad (21)$$

In the $\epsilon \to 0$ limit, the E_0 and G_0 Fourier coefficients should give the Descartes rainbow angle, and the $m = 2$ coefficients should give the first order in ϵ approximation of Eqs. (18) and (19). If the cylinder cross section has twofold symmetry, as is the case for an ellipse, only even Fourier coefficients contribute, as $\theta_p^R(\xi)$ possesses 180° rotational symmetry. For a more general cross-sectional shape lacking twofold symmetry, both even and odd Fourier coefficients are nonzero because $\theta_p^R(\xi)$ possesses only 360° rotational symmetry. Thus the Fourier-series expansion of $\theta_p^R(\xi)$ should provide a sensitive determination of the average ellipticity and the deviation from ellipticity of the cylinder's cross section.

The way in which the cross-sectional shape is encoded into the Fourier coefficients of $\theta_2^R(\xi)$ and $\theta_3^R(\xi)$ was determined in the following two numerical experiments. In the first experiment, we explored the sensitivity of the rainbow angles on the ellipticity of the cylinder cross section. At 1° intervals in ξ, the $p = 2$ and the $p = 3$ deviation angles of a large number of parallel light rays incident upon an elliptical-cross-section cylinder were obtained numerically with our ray-tracing procedure, and the minimum deviation angle (i.e., the rainbow angle) was identified. In Tables 1 and 2 we show the first five even Fourier coefficients of the $p = 2$ and $p = 3$ rainbow angles obtained with this procedure for a cylinder with an elliptical cross section, a refractive index of $n = 1.474$ corresponding to the experimental measurements of Section 3, and ellipticities of $\epsilon = -0.001, -0.01$, and -0.1. Also shown are the $m = 2$ Fourier coefficients corresponding to the first order in ϵ approximation of Eqs. (18) and (19). These tables illustrate the following results. First, as a check of our ray-tracing computer program, the $\epsilon \to 0$ limit of the $m = 0, 2$ Fourier coefficients produced the Descartes rainbow angle and the first order in ϵ elliptical-cross-section approximation of Eqs. (18) and (19), respectively. The Fourier coefficients were found to have the following dependence on ϵ. They converge rapidly as a function of m and are roughly proportional to $|\epsilon|^{m/2}$. As $|\epsilon|$ increases, the $m = 0$ coefficient shifts somewhat and the $m = 2$ coefficients begin to deviate from linearity in ϵ, reflecting the existence of contributions to the coefficients of higher order in ϵ (the order ϵ^2 contribution was analytically calculated in Ref. 16 for $p = 3$ and $n \approx 1.34$). The higher orders in ϵ contributions are larger for the second-order rainbow than they are for the first-order rainbow for $n = 1.474$ and produce roughly similar sensitivities of the two rainbow angles on the ellipticity ϵ. The most important conclusion of our first numerical experiment, however, is that E_0 and G_0 are determined primarily by the cylinder refractive index whereas

Table 1. First Five Even Fourier Coefficients in Degrees of the First-Order Rainbow Deviation Angle $\theta_2^R(\xi)$ for an Elliptical Cross-Sectional Cylinder with Refractive Index $n = 1.474$ and Ellipticities $\epsilon = -0.001, -0.01$, and -0.1 as Defined in Eq. (17)[a]

	ϵ		
Coefficient	-0.001	-0.01	-0.1
E_0	154.723	154.713	153.571
E_2	-0.134	-1.346	-13.421
F_2	-0.063	-0.636	-6.531
E_4	2.3×10^{-4}	0.021	2.104
F_4	-4.1×10^{-5}	-0.005	-0.477
E_6	$<10^{-6}$	-2.9×10^{-4}	-0.296
F_6	$<10^{-6}$	3.2×10^{-4}	0.332
E_8	$<10^{-6}$	$<10^{-6}$	0.015
F_8	$<10^{-6}$	$<10^{-6}$	-0.113
E_2^{Mobius}	-0.134	-1.340	-13.396
F_2^{Mobius}	-0.063	-0.633	-6.325

[a]The coefficients E_2^{Mobius} and F_2^{Mobius} are obtained from Eq. (18). The Descartes rainbow deviation angle is $\theta_2^D = 154.723°$.

Table 2. First Five Even Fourier Coefficients in Degrees of the Second-Order Rainbow Deviation Angle $\theta_3^R(\xi)$ for an Elliptical Cross-Sectional Cylinder with Refractive Index $n = 1.474$ and Ellipticities $\epsilon = -0.001, -0.01$, and -0.1 as Defined in Eq. (17)[a]

	ϵ		
Coefficient	-0.001	-0.01	-0.1
G_0	262.121	262.159	266.370
G_2	0.016	0.160	1.116
H_2	-0.115	-1.162	-13.481
G_4	2.4×10^{-4}	0.021	1.980
H_4	1.9×10^{-4}	0.018	1.730
G_6	$<10^{-6}$	-4.2×10^{-4}	-0.675
H_6	$<10^{-6}$	-9.4×10^{-4}	-0.931
G_8	$<10^{-6}$	$<10^{-6}$	0.009
H_8	$<10^{-6}$	$<10^{-6}$	0.247
G_2^{Mobius}	0.016	0.160	1.599
H_2^{Mobius}	-0.115	-1.155	-11.546

[a]The coefficients G_2^{Mobius} and H_2^{Mobius} are obtained from Eq. (19). The Descartes rainbow deviation angle is $\theta_3^D = 262.121°$.

Table 3. First Six Fourier Coefficients in Degrees of the First-Order Rainbow Deviation Angle $\theta_2^R(\xi)$ for a Two-Half-Ellipse Cross-Sectional Cylinder with Refractive Index $n = 1.474$, Average Ellipticity $\epsilon_{ave} = -0.037$, and Various Values of the Ellipticity Difference $\Delta\epsilon$ as Defined in Eq. (23)

	$\Delta\epsilon$				
Coefficient	0.00	0.01	0.02	0.03	0.04
E_0	154.580	154.580	154.580	154.579	154.577
E_1	0.000	0.039	0.078	0.116	0.154
F_1	0.000	0.011	0.022	0.034	0.044
E_2	−5.019	−5.019	−5.021	−5.023	−5.025
F_2	−2.378	−2.378	−2.378	−2.378	−2.379
E_3	0.000	0.045	0.090	0.136	0.183
F_3	0.000	0.034	0.069	0.104	0.139
E_4	0.293	0.294	0.299	0.307	0.319
F_4	−0.068	−0.066	−0.062	−0.055	−0.046
E_5	0.000	−0.027	−0.054	−0.081	−0.108
F_5	0.000	−0.046	−0.092	−0.137	−0.182

the $m = 2$ coefficients are determined primarily by the cylinder ellipticity.

In the second numerical experiment, we explored the sensitivity of the rainbow angles on the deviation of the cylinder cross section from ellipticity. In Tables 3 and 4 we show the first six Fourier coefficients for the $p = 2$ and the $p = 3$ rainbow angles of a cylinder that has a two-half-ellipse cross section, a refractive index of $n = 1.474$, an average ellipticity

$$\epsilon_{ave} = \frac{(b_1/a) + (b_2/a)}{2} - 1 = \frac{\epsilon_1 + \epsilon_2}{2} \tag{22}$$

of −0.037, corresponding to the experimental measurements of Section 3, and an ellipticity difference

$$\Delta\epsilon = (b_1/a) - (b_2/a) = \epsilon_1 - \epsilon_2 \tag{23}$$

ranging from zero to 0.04, where

$$\epsilon_1 = b_1/a - 1, \qquad \epsilon_2 = b_2/a - 1. \tag{24}$$

Table 4. First Six Fourier Coefficients in Degrees of the Second-Order Rainbow Deviation Angle $\theta_3^R(\xi)$ for a Two-Half-Ellipse Cross-Sectional Cylinder with Refractive Index $n = 1.474$, Average Ellipticity $\epsilon_{ave} = -0.037$, and Various Values of the Ellipticity Difference $\Delta\epsilon$ as Defined in Eq. (23)

	$\Delta\epsilon$				
Coefficient	0.00	0.01	0.02	0.03	0.04
G_0	262.657	262.638	262.619	262.565	262.489
G_1	0.000	−0.011	−0.023	−0.034	−0.046
H_1	0.000	0.034	0.068	0.102	0.134
G_2	0.584	0.579	0.574	0.569	0.561
H_2	−4.420	−4.408	−4.397	−4.381	−4.358
G_3	0.000	0.575	1.150	1.724	2.294
H_3	0.000	0.784	1.669	2.511	3.362
G_4	0.301	0.310	0.320	0.353	0.395
H_4	0.256	0.257	0.259	0.264	0.269
G_5	0.000	0.120	0.240	0.359	0.479
H_5	0.000	−0.168	−0.337	−0.505	−0.670

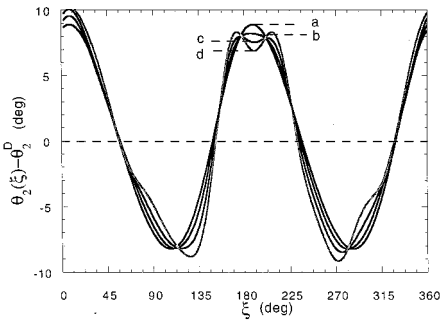

Fig. 3. Deviation of the first-order rainbow angle $\theta_2^R(\xi)$ of a two-half-ellipse cross-section cylinder from the Descartes first-order rainbow angle θ_2^D as a function of the rotation angle ξ for a refractive index $n = 1.474$, average ellipticity $\epsilon_{ave} = 0.060$, and ellipticity difference $\Delta\epsilon = 0$ (curve a), $\Delta\epsilon = 0.06$ (curve b), $\Delta\epsilon = 0.12$ (curve c), and $\Delta\epsilon = 0.18$ (curve d). The range of $\Delta\epsilon$ here is much larger than in Table 3 because the dependence of the rainbow angle on $\Delta\epsilon$ is weak. The value of ϵ_{ave} is also different than that in Table 3.

Tables 3 and 4 illustrate the following results. The 180° rotational symmetry of the second-order rainbow angle is quickly lost for $n = 1.474$ when $\Delta\epsilon$ is nonzero, and the symmetry loss is encoded primarily in the $m = 3$ coefficients. The symmetry loss is much less pronounced for the first-order rainbow because its $m = 3$ coefficients are more than an order of magnitude smaller than those of the second-order rainbow. Evidently the partially compensating changes in the path of the second-order rainbow ray inside an elliptical-cross-section cylinder described in Ref. 16 are easily disturbed when the cylinder surface assumes a less symmetric shape. The values of the even Fourier coefficients remain nearly constant as the ellipticity difference is varied and the average ellipticity is held fixed, and the magnitudes of the odd m coefficients increase roughly linearly in $\Delta\epsilon$. In Figs. 3 and 4 we graph $\theta_2^R(\xi)$ and $\theta_3^R(\xi)$, respectively. If we had used the results of Table 3 in Fig. 3, the various graphs would have been indistinguishable in

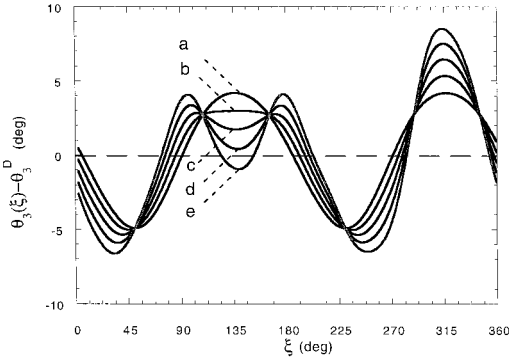

Fig. 4. Deviation of the second-order rainbow angle $\theta_3^R(\xi)$ for a two-half-ellipse cross-section cylinder from the Descartes second-order rainbow angle θ_3^D as a function of the rotation angle ξ for a refractive index $n = 1.474$, average ellipticity $\epsilon_{ave} = -0.037$, and ellipticity difference $\Delta\epsilon = 0$ (curve a), $\Delta\epsilon = 0.01$ (curve b), $\Delta\epsilon = 0.02$ (curve c), $\Delta\epsilon = 0.03$ (curve d), and $\Delta\epsilon = 0.04$ (curve e). These parameters are identical to those of Table 4.

the figure because the first-order rainbow angle depends only weakly on $\Delta\epsilon$. Thus we consider a much larger range of $\Delta\epsilon$ in Fig. 3. In Fig. 4, on the other hand, we graph the results of Table 4. In Fig. 3, the first-order rainbow angle appears to be independent of $\Delta\epsilon$ for eight cylinder rotation angles ξ, whereas in Fig. 4 for the second-order rainbow, there appear to be six such angles. The reason for this is at present unknown, although we speculate that these invariant points are a consequence of the reflection symmetry of the two-half-ellipse cross section about the y' axis. Last, the behavior of the Fourier coefficients when ϵ_{ave} is either positive (as in Fig. 3) or negative (as in Fig. 4) is qualitatively similar.

The tables and the figures derived from our two numerical experiments demonstrate for $n = 1.474$ that (1) the first- and the second-order rainbow angles have similar sensitivities to the average ellipticity of the cylinder cross section, (2) because the second-order rainbow is far more sensitive to the ellipticity difference than is the first-order rainbow, observation of the second-order rainbow provides a sensitive test for deviations of the cylinder cross section from ellipticity, and (3) the refractive index, the average ellipticity, and the ellipticity difference are encoded primarily in the $m = 0$, 2, 3 Fourier coefficients, respectively.

3. Experiment

Light-scattering experiments were performed on a glass rod of length 13.4 ± 0.05 cm and with a nearly circular cross section of nominal diameter 16 mm. We had previously estimated the refractive index and the average ellipticity of the rod to be $n = 1.484$ and $\epsilon_{ave} = 0.04$, respectively.[5,19] In the present experiment, the rod was mounted on a calibrated rotation stage whose axis coincided with the rod's major axis. The $\lambda = 0.6328$ μm unpolarized beam of a 15-mW He–Ne laser was expanded to a 5.0-cm diameter by a series of lenses and was normally incident upon the rod. Coincidence of the rotation stage axis and the rod's major axis was ensured by requiring that the shadow of the rod on a viewing screen 3 m away remain stationary as the rod was rotated.

In order to obtain a more accurate estimate of the rod's refractive index and ellipticity than we had previously made, we measured the scattering angle of the first- and the second-order rainbows to an accuracy of $\pm 0.05°$ (i.e., the width of the principal Airy peak) as the rod was rotated in 5° increments. The first-order rainbow was measured 89 cm away from the rod axis and the second-order rainbow was measured 48 cm away. To ensure that local inhomogeneities or inclusions in the glass were not strongly affecting our results, measurements of the $p = 2$ and the $p = 3$ rainbow angles were made at two different points, separated by 8 cm, along the rod's major axis. Our results for both sets of measurements were identical to within $\pm 0.1°$. Additional qualitative evidence for the lack of large inhomogeneities is provided by the fact that the rainbows and their supernumeraries, as seen on the viewing screen, were

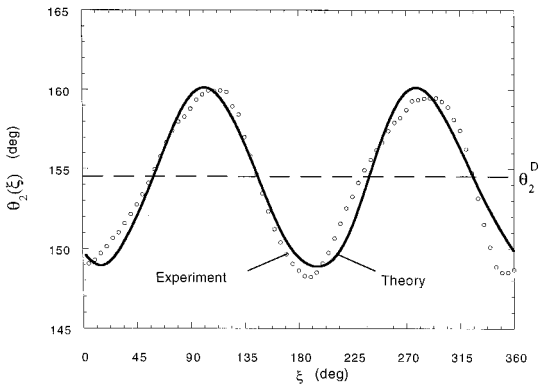

Fig. 5. Experimental first-order rainbow deviation angle as a function of the rotation angle ξ and the theoretical fit of the two-half-ellipse cross-section model with $n = 1.474$, $\epsilon_{ave} = -0.037$, and $\Delta\epsilon = 0.026$.

straight lines parallel to the rod's major axis, rather than curving back and forth, as was the case for other less carefully manufactured glass and plastic rods we had previously examined. Because the rainbow angles were measured less than 100 radii from the rod, we corrected the data to the far zone by taking into account the near-zone curvature of the rainbow caustics by using the method outlined in the Appendix of Ref. 20. The correction produced a systematic 0.40° shift for the first-order rainbow angle and a systematic 0.89° shift for the second-order rainbow angle. The corrected experimental data are shown in Figs. 5 and 6. A Fourier-series decomposition of the corrected data was also performed and the first six Fourier coefficients are given in Tables 5 and 6.

As is seen in Figs. 5 and 6, both the first- and the second-order rainbow angles were not stationary as the rod was rotated, indicating that the rod's cross section is not circular. Further, the second-order rainbow data clearly do not possess 180° rotational symmetry, indicating that the rod's cross section does not possess twofold symmetry. The first-order rainbow data also do not possess 180° rotational symmetry, but the effect is smaller, as is expected from the

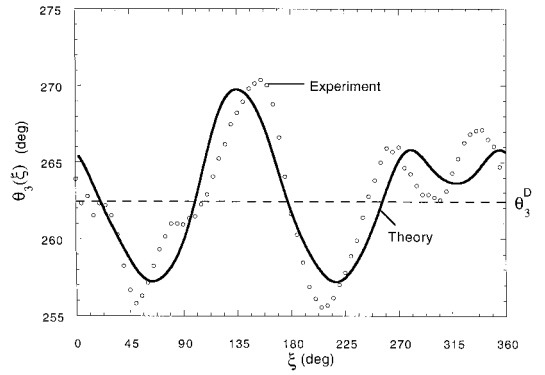

Fig. 6. Experimental second-order rainbow deviation angle as a function of the rotation angle ξ and the theoretical fit of the two-half-ellipse cross-section model with $n = 1.474$, $\epsilon_{ave} = -0.037$, and $\Delta\epsilon = 0.026$.

Table 5. First Six Fourier Coefficients in Degrees of the Experimental First-Order Rainbow Deviation Angle and of $\theta_2^R(\xi)$ for a Cylinder with a Two-Half-Ellipse Cross Section, Refractive Index $n = 1.474$, Average Ellipticity $\epsilon_{ave} = -0.037$, and Ellipticity Difference $\Delta\epsilon = 0.026$

Fourier Coefficient	Experiment	Theory
E_0	153.990	154.579
E_1	−0.071	0.101
F_1	0.063	0.029
E_2	−5.217	−5.022
F_2	−1.909	−2.378
E_3	0.131	0.118
F_3	0.129	0.090
E_4	−0.721	0.303
F_4	0.514	−0.058
E_5	−0.061	−0.071
F_5	0.314	−0.119

analysis of Section 2. Assuming for the moment that the rod's cross section was elliptical (i.e., $\Delta\epsilon = 0$), the numerical ray-tracing method of Section 2 was used to preliminarily fit the $m = 0, 2$ Fourier coefficients of the experimental data. The orientation of the widest part of the rod's cross section could not be visually determined to any better than $\pm 5°$ when the rod was placed on the rotation stage, and, as a result, some uncertainty in the $\xi = 0°$ orientation of the rod was produced. Thus the quantities $(E_2^2 + F_2^2)^{1/2}$ and $(G_2^2 + H_2^2)^{1/2}$ were fitted rather than the individual Fourier coefficients because translations of the data along the ξ axis, corresponding to different choices for the $\xi = 0°$ orientation of the rod, affect only the phase angle of the Fourier coefficients for a given value of m while keeping the magnitude constant. The magnitudes of the experimental first- and second-order rainbow $m = 0, 2$ Fourier coefficients were numerically fitted equally well by $n = 1.474 \pm 0.002$ and $\epsilon = \pm 0.038 \pm 0.001$. The two ellipticities, differing by only a minus sign, correspond to a rotation of the $\xi = 0°$ orientation of the ellipse by 90°. Our previous refractive-index estimate[19] is less precise than the present measurement because the second-order rainbow angle depends sensitively on ξ when $\theta_3^R \approx \theta_3^D$. Thus a possible slight misalignment of the rod in our previous measurement, made when $\theta_3^R \approx \theta_3^D$, would have had significant consequences.

Table 6. First Six Fourier Coefficients in Degrees of the Experimental Second-Order Rainbow Angle and of $\theta_3^R(\xi)$ for a Cylinder with a Two-Half-Ellipse Cross Section, Refractive Index $n = 1.474$, Average Ellipticity $\epsilon_{ave} = -0.037$, and Ellipticity Difference $\Delta\epsilon = 0.026$

Fourier Coefficient	Experiment	Theory
G_0	262.673	262.587
G_1	−0.103	−0.030
H_1	−0.283	0.092
G_2	0.500	0.570
H_2	−4.287	−4.389
G_3	1.404	1.491
H_3	2.093	2.177
G_4	0.645	0.342
H_4	−1.908	0.267
G_5	−0.220	0.314
H_5	0.380	−0.439

Once the $m = 0, 2$ Fourier coefficients were estimated, the ellipticity difference $\Delta\epsilon$ was varied in our numerical ray-tracing method, and the refractive index and the average ellipticity were slightly adjusted from their previously obtained values until the experimental Fourier coefficient magnitudes $(E_3^2 + F_3^2)^{1/2}$ and $(G_3^2 + H_3^2)^{1/2}$, along with E_0, G_0, $(E_2^2 + F_2^2)^{1/2}$, and $(G_2^2 + H_2^2)^{1/2}$, were matched as well as possible. Both the first- and the second-order rainbow Fourier coefficient magnitudes were numerically fitted well by $n = 1.474 \pm 0.002$, $\epsilon_{ave} = -0.037 \pm 0.001$, and $\Delta\epsilon = 0.026 \pm 0.001$. The theoretical fits are shown in Figs. 5 and 6, and the first six theoretical Fourier coefficients are given in Tables 5 and 6. The correspondence in Figs. 5 and 6 is not perfect, as the actual shape of the rod's cross section is not exactly that of two half-ellipses smoothly joined on the x' axis. This is evidenced by our inability to match exactly both the smaller $m = 1$ and $m \geq 4$ Fourier coefficients (in a few cases even the signs are incorrect) and to match simultaneously all the phases of the dominant $m = 2, 3$ coefficients. But all in all, the two-half-ellipse model did a good job of reproducing the major features of the experimental data, especially the double oscillation of the second-order rainbow angle in the range $250° \leq \xi \leq 360°$. A good fit of the $m = 0, 2, 3$ Fourier coefficients for both rainbows with a single n, ϵ_{ave}, and $\Delta\epsilon$ is also an encouraging sign. Finally, after the experimental data was fitted, the largest and the smallest diameters of the rod's cross section were measured with a micrometer and were found to be 16.414 ± 0.01 mm and 15.794 ± 0.01 mm, respectively, giving $\epsilon_{ave} = -0.0378 \pm 0.0006$, in agreement with the value determined by the Fourier coefficient matching method.

We then measured the angular positions of the supernumeraries of the first-order rainbow for a representative rod rotation angle by masking a photodetector with a 0.1-mm slit aperture and advancing its position in 0.013-mm increments with a calibrated stepper motor. An angular scan of the light intensity in the vicinity of the first-order rainbow is shown in Fig. 7. Because the aperture slit was wide com-

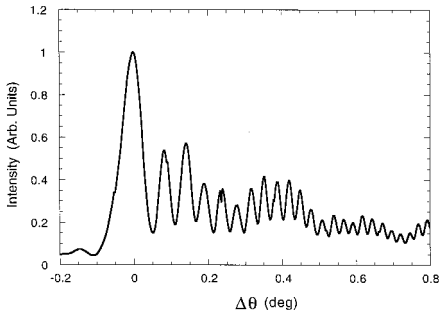

Fig. 7. Experimental light intensity I in the vicinity of the first-order rainbow as a function of scattering angle $\Delta\theta$. The peak of the principal rainbow maximum corresponds to $\Delta\theta = 0°$.

pared with the increment step, the scan somewhat blurred the rainbow features, reduced the rainbow signal with respect to the background scattered light, and eliminated the high-spatial-frequency structure caused by the interference of the $p = 2$ rays with the $p = 0$ specularly reflected rays.[21] But it did not shift the positions of the supernumerary maxima and minima. We obtained an estimate of the rod diameter by fitting the angular positions of the relative maxima and minima of the data with the maxima and the minima of the square of an Airy function.[22] The average diameter obtained from the first four maxima and the first four minima of the experimental data is 23.6 ± 0.5 mm, which is 47% higher than the actual average diameter. Previous comparisons of the supernumerary positions with Airy theory for a pendant water droplet with a 2-mm horizontal diameter did not show such a discrepancy.[23]

This large discrepancy was not unanticipated, however. As we rotated the rod through a complete revolution, we noted that the supernumerary structure of both the first- and the second-order rainbows alternately expanded and contracted by a factor of ~2. On the other hand, the largest and the smallest diameters of the rod's cross section differ by only 3.8%. Thus one would expect that, as the argument of the Airy function is proportional to $a^{2/3}$ for a circular-cross-section cylinder (where a is the cylinder radius), the supernumerary pattern should expand and contract by only 2.5%. But for a circular-cross-section cylinder in Airy theory, the argument of the Airy function also depends on $h^{-1/3}$, in which the parameter h depends on p and the refractive index,[22] and describes the angular spreading of the outgoing flux tube of scattered rays in the vicinity of the $p - 1$-order rainbow. The angular spreading rate depends on the curvature of the cylinder surface at the ray interaction points. As a result, the observed variation of the width of the supernumerary pattern as the rod was rotated may well reflect a corresponding variation in the flux tube angular spreading rate. This was not an issue for the experiment of Ref. 23, in which the horizontal cross section of the pendant droplet was circular. To test this flux tube variation hypothesis, it would be of interest to extend Airy theory to an elliptical-cross-section cylinder. We also observed the fourth-order rainbow in the vicinity of the second-order rainbow and the fifth-order rainbow near backscattering. The details of our higher-order rainbow observations are presented separately.[24]

4. Visibility of the Supernumeraries of the Second-Order Rainbow

In rain showers, the topmost portions of the first- and the second-order rainbows are produced by light scattered in the vertical plane of the approximately oblate spheroidal falling water droplets. In the vertical plane, the droplet cross section is nearly elliptical, with $|\epsilon_{ave}|$ increasing as the equal-volume-sphere radius a_0 increases. But as was seen in Section 2, the deviation angles of the first- and the second-order rainbows depend on both $|\epsilon_{ave}|$ and on the orientation of the incident light rays with respect to the ellipse. This ellipticity-produced shift in the rainbow angle with respect to the Descartes angle, along with the Airy theory prediction that the shift in the rainbow angle with respect to the Descartes angle decreases as a_0 increases, influences the observability of the supernumeraries at the topmost portion of the first and second order rainbows. For the first-order rainbow, the ellipticity-produced shift increases as a_0 increases and balances the decreasing shift predicted by Airy theory. The balancing produces a relative minimum of the deviation angle when $a_0 \approx 0.25$ mm, which is responsible for the observability of the first few supernumeraries at the topmost portion of the first-order rainbow.[15] On the other hand, observations of the supernumeraries of the second-order rainbow are exceedingly rare.[25,26] The much smaller ellipticity-produced shift of the second-order rainbow for $n = 1.333$ balances the Airy theory shift when $a_0 \approx 0.7$ mm for a narrow range of solar elevation angles, rendering the first one or two supernumeraries at the topmost portion of the second order rainbow potentially observable under only certain special circumstances.[16]

Hydrodynamic forces produce an increased flattening of the lower surface of water droplets falling at terminal velocity, causing the cross section in the vertical plane to deviate from ellipticity. The two-half-ellipse model of Section 2 should closely approximate the major features of the actual shape of a water droplet's vertical cross section. We calculated the values of b_1/a and b_2/a, and from them the ellipticity ϵ_{ave} and the ellipticity difference $\Delta\epsilon$ for a number of equivalent-sphere-radius water droplets by using the Fourier-series parameterization of Table 2 of Ref. 14. The results are shown in Fig. 8. Also shown in Fig. 8 are an analytical approximation to ϵ_{ave} derived in Ref. 27 and a linearization of it used in Ref. 16. It is interesting that for a_0 as small as 0.35 mm, the ellipticity difference is larger than 10% of the average ellipticity, and for $a_0 \geq 0.62$ mm, $\Delta\epsilon$ is more than 20% of ϵ_{ave}.

Our numerical ray-tracing method shows that the deviation angle of the first-order rainbow again depends strongly on ϵ_{ave} and only weakly on $\Delta\epsilon$ for $n = 1.333$. Thus no change is produced in the observability of the supernumeraries of the first-order rainbow. But the shift in the deviation angle of the second-order rainbow for the refractive index of water depends only weakly on ϵ_{ave}, as the first order in ϵ approximation of Eq. (19) vanishes for $n = 1.342$. As a result, almost all the ellipticity-produced shift is due to terms of higher order in ϵ_{ave}, which are small for $n = 1.333$ and $|\epsilon_{ave}| \leq 0.1$, corresponding to falling water droplets of radii $a_0 \leq 1.2$ μm. The shift in the deviation angle of the second-order rainbow, however, again depends linearly on $\Delta\epsilon$ for $n = 1.333$, with the result that the nonellipticity-produced shift can easily exceed the ellipticity-produced shift for water droplets of the size that are found in rain showers.[28] Thus the increased flattening of the lower surface of the falling droplets should have a strong influence on the observability of

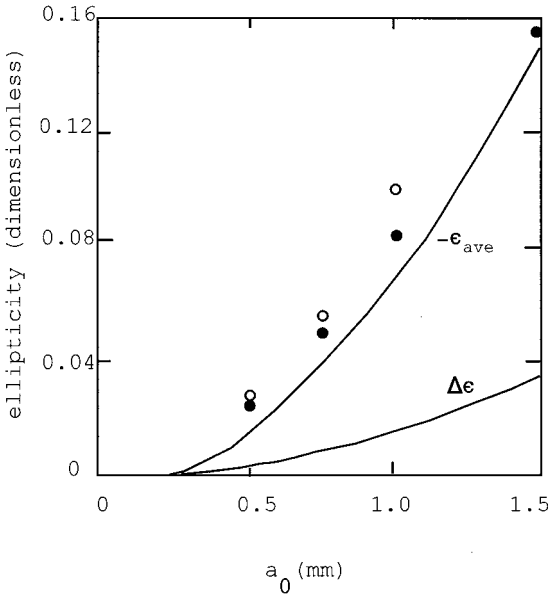

Fig. 8. Negative of the average ellipticity $-\epsilon_{ave}$ and the ellipticity difference $\Delta\epsilon$ as functions of the equal-volume-sphere radius a_0 of raindrops falling at terminal velocity and derived from the parameterization of Ref. 14. The filled circles are the analytical approximation to $-\epsilon_{ave}$ of Ref. 27, and the open circles are the linearized approximation of Ref. 16.

the topmost portion of the first few supernumeraries of the second-order rainbow.

We then computed the second-order rainbow deviation angle for $n = 1.333$ by using the numerical ray-tracing approach of Section 2 for a number of equal-volume-sphere radii in the range $0.17 \text{ mm} \leq a_0 \leq 1.5 \text{ mm}$ for various solar angles between 0° and 40° and by using the values of ϵ_{ave} and $\Delta\epsilon$ given in Fig. 8. As mentioned above, the second-order rainbow angle in general shifted by an equal or greater amount between the two-half-ellipse cross-section condition ($\epsilon_{ave} \neq 0$, $\Delta\epsilon \neq 0$) and the elliptical-cross-section condition ($\epsilon_{ave} \neq 0$, $\Delta\epsilon = 0$) than it did between the elliptical-cross-section condition and the spherical-cross-section condition ($\epsilon_{ave} = 0$, $\Delta\epsilon = 0$). When added to the Airy theory shift, the resulting second-order rainbow deflection angle as a function of a_0 is shown in Figs. 9(a), 9(b), and 9(c) for solar elevation angles of 10° (i.e., low Sun), 20° (i.e., moderate elevation), and 40° (i.e., high Sun), respectively.

For a solar elevation of 10°, the nonellipticity-produced shift in the second-order rainbow deflection angle is sufficiently large to cause the angle to have a rather narrow relative minimum at $a_0 \approx 0.38$ mm for the principal peak, at $a_0 \approx 0.65$ mm for the first supernumerary, and at $a_0 \approx 0.70$ mm for the second supernumerary. In a typical rain shower[28] there is over an order of magnitude fewer raindrops with radii $0.65 \text{ mm} \leq a_0 \leq 0.70 \text{ mm}$ than with $0.23 \text{ mm} \leq a_0 \leq 0.28$ mm, which correspond to the relative minimum droplet radii for the first two supernumeraries of the first-order rainbow.[15] The combination of fewer contributing droplets, the reduced brightness of the second-order rainbow with respect to the first-

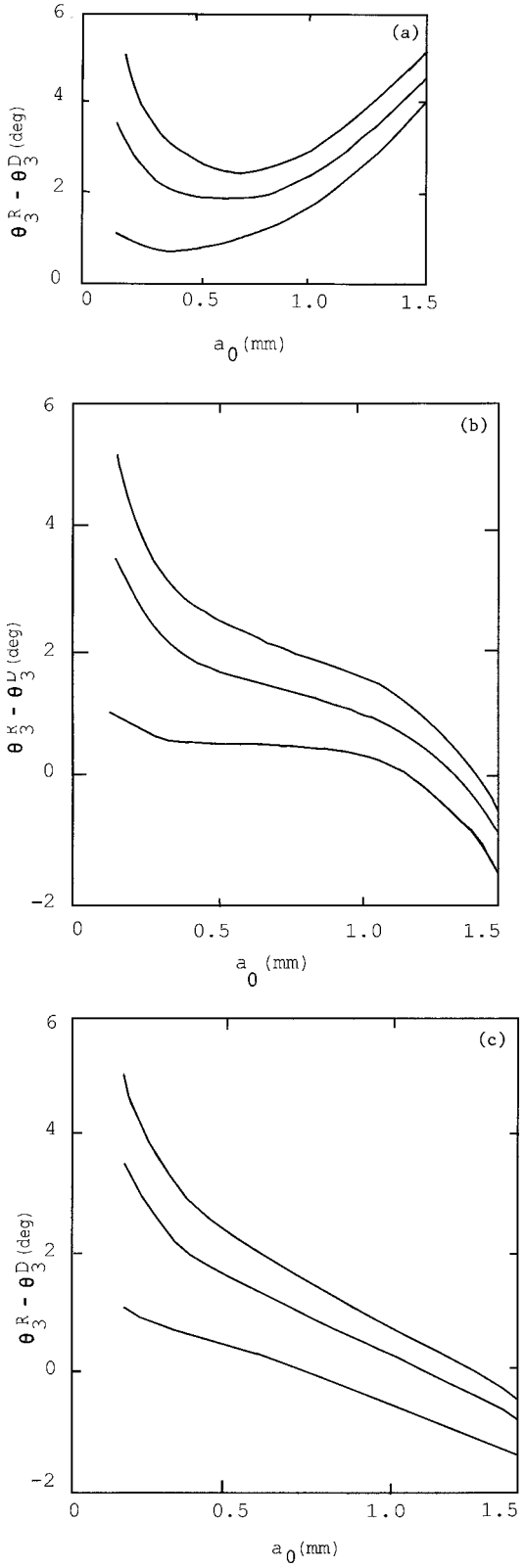

Fig. 9. Deviation angle of the second-order rainbow $\theta_3{}^R$ with respect to the Descartes second-order rainbow angle $\theta_3{}^D$ as a function of the equal-volume-sphere radius a_0 of raindrops falling at terminal velocity for solar elevation angles of (a) 10°, (b) 20°, (c) 40°. In each graph, the lowest curve is the principal Airy maximum, the middle graph is the first supernumerary maximum, and the highest curve is the second supernumerary maximum.

order rainbow due to the extra internal reflection, and the brightness of the background sky above the second-order rainbow, provide major reasons for the extreme rarity of observations of supernumeraries of the second-order rainbow.[25,26] At solar elevation angles of 20° and 40°, Figs. 9(b) and 9(c), respectively, show that the nonellipticity-produced shift is sufficiently large to cause the second-order rainbow deviation angle not to possess a relative minimum, suggesting great difficulty in second-order rainbow supernumerary formation at moderate and high solar elevation angles.

There are, however, three caveats to these predictions. First, although we found that the deviation angle of the second-order rainbow depends sensitively on $\Delta\epsilon$ for $n = 1.333$ in the two-half-ellipse model, the vertical cross section of a water droplet is only approximately modeled by two half-ellipses smoothly joined together on the x' axis. In particular, the radius of curvature of a water droplet is continuous everywhere, whereas it is discontinuous at the join points in the two-half-ellipse model. As a result, more refined modeling of the droplet surface might produce additional nonellipticity-produced shifting of the second-order rainbow deviation angle. In order to examine this possibility, it would be of interest to derive the formulas for the $p - 1$-order rainbow angle when the shape of the vertical cross section in polar coordinates is given by a Fourier series, so that direct contact can be made with the surface shape parameterization of Ref. 14. Second, there is more to rainbow observability than merely the existence or nonexistence of a relative minimum of the rainbow deflection angle as in Fig. 9(a). In particular, the raindrop size distribution, which is different from one rain shower to the next and at different heights above the ground in a given shower,[29] must be integrated over because the rainbow intensity is proportional to ${a_0}^{7/3}$ in Airy theory. Also, the rainbow colors become less saturated when the intensity pattern is integrated over the angular extent of the solar disk. These refinements were included in Ref. 16 for oblate spheroidal water droplets. Third, the supernumeraries of the second-order rainbow can be observed in a rain shower or an artificially made spray whose raindrop size distribution is quite narrow, even if the rainbow deviation angle is a strictly decreasing function of a_0, as is the case in Figs. 9(b) and 9(c). This may well explain the visibility of the first supernumerary of the second-order rainbow in the photographs of artificially made sprays, as described in Ref. 16.

5. Discussion

Our principal result is that the refractive index, average ellipticity, and ellipticity difference of a glass fiber or rod can be accurately determined by fitting the Fourier coefficients of its second-order rainbow angle taken as a function of the rod's rotation angle. In our experiment, this optical method fit the average ellipticity of the rod quite well when compared with micrometer measurements. Theoretically the $m = 3$ Fourier coefficients were found to depend sensitively on $\Delta\epsilon$ for the second-order rainbow. Specifically, in the region of parameter space corresponding to our glass rod, the magnitude of the $m = 3$ coefficient changes by 5% when $\Delta\epsilon$ changes by 0.001. A change in $\Delta\epsilon$ of 0.001 corresponds to a 16-μm change in the largest and the smallest diameters when the average rod diameter is 16.1 mm. Resolution of distances of the order of a number of micrometers usually requires interferometric techniques. It can be argued that observing the rainbow is an interferometric technique, as the rainbow occurs at the confluence of the two ray paths that produce the supernumerary interference pattern. Because Mie calculations exhibit both a well-defined second-order rainbow and supernumeraries for a circular-cylinder size parameter of the order of a few hundred,[22] this technique should remain feasible for fiber diameters to as low as ~40 μm.

References

1. C. B. Boyer, *The Rainbow From Myth to Mathematics* (Princeton U. Press, Princeton, N.J., 1987), p. 309.
2. W. Möbius, "Zur Theorie des Regenbogens und ihrer experimentallen Prüfung," Abh. Kgl. Saechs. Ges. Wiss. Math.-Phys. Kl. **30,** 105–254 (1907–1909).
3. W. Möbius, "Zur Theorie des Regenbogens und ihrer experimentallen Prüfung," Ann. Phys. **33,** 1493–1558 (1910).
4. H. M. Presby, "Refractive index and diameter measurements of unclad optical fibers," J. Opt. Soc. Am. **64,** 280–284 (1974).
5. J. A. Lock and C. L. Adler, "Debye-series analysis of the first-order rainbow produced in scattering of a diagonally incident plane wave by a circular cylinder," J. Opt. Soc. Am. A **14,** 1316–1328 (1997).
6. P. L. Marston, "Descartes glare points in scattering by icicles: color photographs and a tilted dielectric cylinder model of caustic and glare-point evolution," Appl. Opt. **37,** 1551–1556 (1998).
7. C. M. Mount, D. B. Thiessen, and P. L. Marston, "Scattering observations for tilted transparent fibers: evolution of Airy caustics with cylinder tilt and the caustic-merging transition," Appl. Opt. **37,** 1534–1539 (1998).
8. H. C. van de Hulst, *Light Scattering by Small Particles* (Dover, New York, 1981), pp. 297–328.
9. J. A. Lock, "Scattering of a diagonally incident focused Gaussian beam by an infinitely long homogeneous circular cylinder," J. Opt. Soc. Am. A **14,** 640–652 (1997).
10. G. Gouesbet, "Scattering of a first order Gaussian beam by an infinite cylinder with arbitrary location and arbitrary orientation," Part. Part. Syst. Charact. **12,** 242–256 (1995).
11. P. Morse and H. Feshbach, *Methods of Theoretical Physics* (McGraw-Hill, New York, 1953), pp. 1407–1423.
12. J. J. Bowman, T. B. A. Senior, and P. L. E. Uslenghi, *Electromagnetic and Acoustic Scattering by Simple Shapes* (Hemisphere, New York, 1987), pp. 129–180.
13. J. P. Barton, "Electromagnetic-field calculations for irregularly shaped, layered cylindrical particles with focused illumination," Appl. Opt. **36,** 1312–1319 (1997).
14. H. R. Pruppacher and R. L. Pitter, "A semi-empirical determination of the shape of cloud and rain droplets," J. Atmos. Sci. **28,** 86–94 (1971).
15. A. B. Fraser, "Why can the supernumerary bows be seen in a rain shower?" J. Opt. Soc. Am. **73,** 1626–1628 (1983).
16. G. P. Können, "Appearance of supernumeraries of the secondary bow in rain showers," J. Opt. Soc. Am. A **4,** 810–816 (1987).

17. S. D. Gedzelman, "Rainbows in strong vertical atmospheric fields," J. Opt. Soc. Am. A **5,** 1717–1721 (1988).
18. D. Marcuse, "Light scattering from elliptical fibers," Appl. Opt. **13,** 1903–1905 (1974).
19. C. L. Adler, J. A. Lock, B. R. Stone, and C. J. Garcia, "High-order interior caustics produced in scattering of a diagonally incident plane wave by a circular cylinder," J. Opt. Soc. Am. A **14,** 1305–1315 (1997).
20. J. A. Lock and T. A. McCollum, "Further thoughts on Newton's zero-order rainbow," Am. J. Phys. **62,** 1082–1089 (1994).
21. P. L. Marston, "Rainbow phenomena and the detection of nonsphericity in drops," Appl. Opt. **19,** 680–685 (1980).
22. E. A. Hovenac and J. A. Lock, "Assessing the contributions of surface waves and complex rays to far-field Mie scattering by use of the Debye series," J. Opt. Soc. Am. A **9,** 781–795 (1992).
23. K. Sassen, "Angular scattering and rainbow formation in pendant drops," J. Opt. Soc. Am. **69,** 1083–1089 (1979).
24. J. A. Lock, C. L. Adler, B. R. Stone, and P. D. Zajak, "Amplification of high-order rainbows of a cylinder with an elliptical cross section," Appl. Opt. **37,** 1527–1533 (1998).
25. M. Minnaert, *Light and Colour in the Open Air* (Dover, New York, 1954), p. 173.
26. R. Greenler, *Rainbows, Halos, and Glories* (Cambridge U. Press, Cambridge, 1989), p. 20.
27. A. W. Green, "An approximation for the shapes of large raindrops," J. Appl. Meteorol. **14,** 1578–1583 (1975).
28. H. R. Pruppacher and J. D. Klett, *Microphysics of Clouds and Precipitation* (Reidel, Dordrecht, The Netherlands, 1978), pp. 23–25.
29. A. B. Fraser, "Chasing rainbows," Weatherwise **36,** 280–289 (1983).